Lab on a Chip

Multimodal detection of protein isoforms and nucleic acids from low starting cell numbers

Journal:	*Lab on a Chip*
Manuscript ID	LC-ART-01-2021-000073.R2
Article Type:	Paper
Date Submitted by the Author:	27-Apr-2021
Complete List of Authors:	Rosas, Elisabet; University of California Berkeley, Bioengineering; Modzelewski, Andrew; University of California Berkeley, Division of Cellular and Developmental Biology, Department of Molecular & Cell Biology Gomez Martinez, Ana; University of California Berkeley, Bioengineering Geldert, Alisha; University of California Berkeley Gopal, Anjali; University of California Berkeley, Bioengineering He, Lin; University of California Berkeley, Division of Cellular and Developmental Biology, Department of Molecular & Cell Biology Herr, Amy; University of California, Berkeley, Department of Bioengineering
Note: The following files were submitted by the author for peer review, but cannot be converted to PDF. You must view these files (e.g. movies) online.	
Author consent.zip	

Article

Multimodal detection of protein isoforms and nucleic acids from low starting cell numbers

Received 00th January 20xx,
Accepted 00th January 20xx

DOI: 10.1039/x0xx00000x

Elisabet Rosàs-Canyelles,[a,b] Andrew J. Modzelewski,[c] Ana E. Gomez Martinez,[a,b] Alisha Geldert,[a,b] Anjali Gopal,[a,b] Lin He,[c] Amy E. Herr[a,b,d,†]

Protein isoforms play a key role in disease progression and arise from mechanisms involving multiple molecular subtypes, including DNA, mRNA and protein. Recently introduced multimodal assays successfully link genomes and transcriptomes to protein expression landscapes. However, the specificity of the protein measurement relies on antibodies alone, leading to major challenges when measuring different isoforms of the same protein. Here we utilize microfluidic design to perform same-cell profiling of DNA, mRNA and protein isoforms (triBlot) on low starting cell numbers (1-100s). After fractionation lysis, cytoplasmic proteins are resolved by molecular mass during polyacrylamide gel electrophoresis (PAGE), adding a degree of specificity to the protein measurement, while nuclei are excised from the device in sections termed "*gel pallets*" for subsequent off-chip nucleic acid analysis. By assaying TurboGFP-transduced glioblastoma cells, we observe a strong correlation between protein expression prior to lysis and immunoprobed protein. We measure both mRNA and DNA from retrieved nuclei, and find that mRNA levels correlate with protein abundance in TurboGFP-expressing cells. Furthermore, we detect the presence of TurboGFP isoforms differing by an estimated <1kDa in molecular mass, demonstrating the ability to discern different proteoforms with the same antibody probe. By directly relating nucleic acid modifications to protein isoform expression in 1-100s of cells, the triBlot assay holds potential as a screening tool for novel biomarkers in diseases driven by protein isoform expression.

[a.] *Department of Bioengineering, University of California, Berkeley, Berkeley, CA 94720, USA.*
[b.] *The UC Berkeley-UCSF Graduate Program in Bioengineering, University of California, Berkeley, CA 94720, USA.*
[c.] *Division of Cellular and Developmental Biology, Department of Molecular & Cell Biology, University of California, Berkeley, Berkeley, CA 94720, USA.*
[d.] *Chan Zuckerberg Biohub. 499 Illinois St, San Francisco, CA 94158, USA.*
† Corresponding author, aeh@berkeley.edu.

Introduction

The discovery of biomarkers for early detection, diagnosis, and therapy remains a persistent challenge across all fields of medicine[1–4]. Protein isoforms are prevalent disease-specific markers and can arise from a variety of events that involve DNA, mRNA and protein, including single nucleotide polymorphisms (SNPs), alternative splicing, or post-translational modifications (PTMs)[5–9]. Many studies have focused on identifying novel potential protein targets by inferring proteoforms from disease-specific modifications to DNA or mRNA[1,7]. However, confirming if DNA or mRNA modifications encode protein isoforms that can become potential diagnostic or therapeutic targets requires multimodal assays that measure all molecules that are produced.

Because DNA, RNA, and protein molecules are the conduit for cellular-level information flow via the "central dogma", simultaneous, same-sample detection of multiple molecular species can provide new insight[10,11]. At the protein level, multimodal analysis is key to understanding gene regulatory networks and the source of variations in both the abundance and molecular forms of proteins expressed. For example, to understand mechanisms of over- or under-expression, multimodal measurements can ascertain the impact of DNA copy number variations on mRNA and protein expression levels[12–14]. In another example, combining proteoform measurements with upstream DNA and RNA measurements can indicate whether proteoforms arise from DNA modifications, alternative RNA splicing, or PTMs. In addition to informing study of gene regulatory networks, multimodal measurements can facilitate more accurate cell subtype classification and lineage tracing[15–17].

Recently introduced technologies allow interrogation of the genome, epigenome, transcriptome, metabolome and proteome at single-cell resolution[18–27]. Multimodal tools that measure proteins and DNA and/or RNA from single cells allow

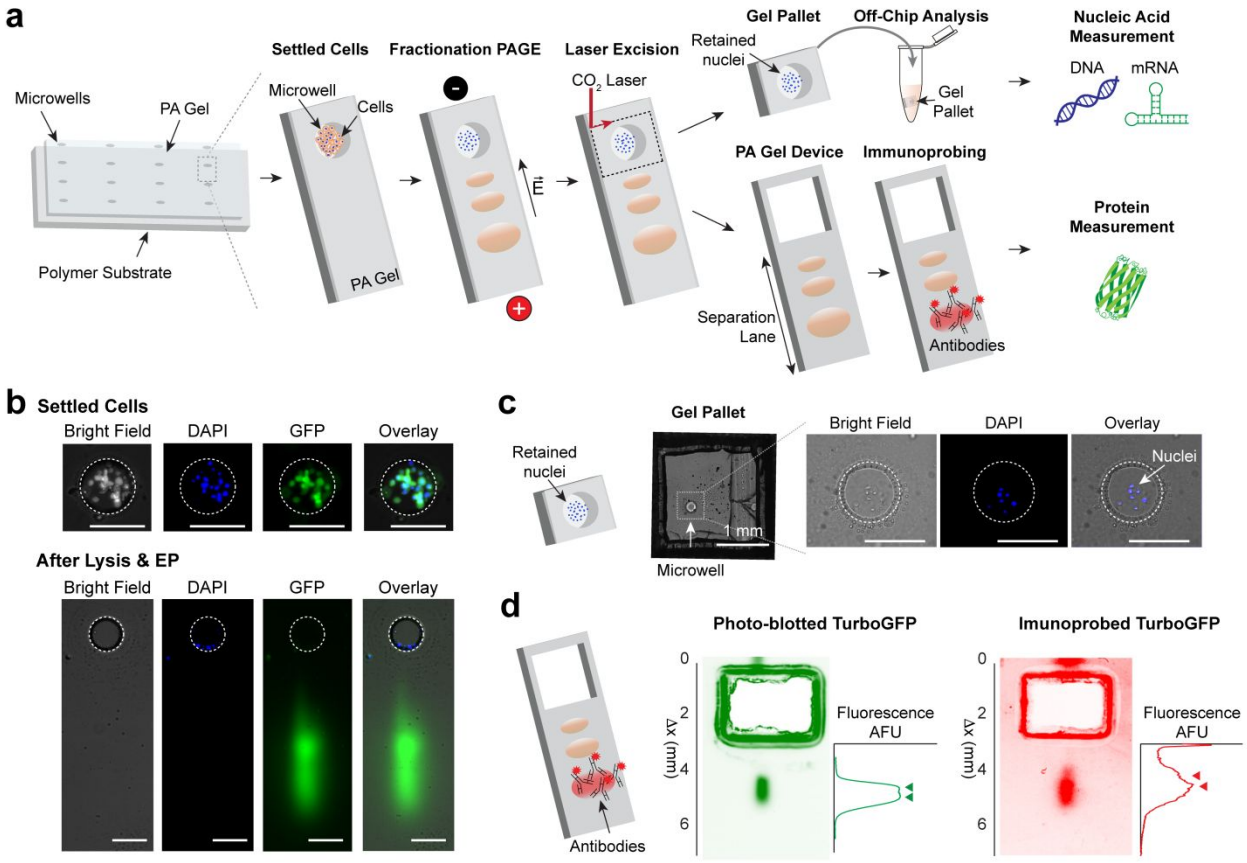

Figure 1 Multimodal measurements by fractionation PAGE coupled with laser excision of microwells into gel pallets for off-chip analysis of nucleic acids. (a) The same-cell nucleic acid and protein isoform immunoblotting device (triBlot) comprises a thin polyacrylamide (PA) gel covalently grafted to a polymer film and stippled with microwells. One to ~200 cells are settled into each microwell of the triBlot device and lysed with a fractionation lysis buffer. Application of an electric field injects the solubilized cytoplasmic proteins into the PA gel for separation by molecular mass. After protein sizing, the proteins are immobilized to the gel by UV-mediated activation of benzophenone that is polymerized into the PA gel matrix. A CO_2 laser excises 2 mm x 3 mm gel sections circumscribing each nuclei-laden microwell, creating gel pallets that are suitable for off-chip for DNA or mRNA analysis. Each protein sizing lane of the planar triBlot device is immunoprobed with fluorescently labeled antibody probes, yielding protein immunoblots indexed to each excised gel pallet. (b) Fractionation PAGE retains nuclei in microwells. Top row displays bright field, DAPI and GFP micrographs of TurboGFP-U251 cells settled into a microwell, prior to the cell lysis step. On bottom, bright field, Hoechst and GFP fluorescence micrographs of microwell and abutting PA gel (separation lane) after fPAGE, when cytoplasmic proteins have been electrophoresed into the PA gel while nuclei remain in the microwell. (c) Gel pallets allow extraction of nuclei for off-chip analysis of nucleic acids. Bright field micrograph shows one gel pallet. Retention of nuclei can be verified by the fluorescence imaging of the Hoechst-stained nuclei, as displayed in the merged micrographs of a gel pallet microwell. (d) Immunoblots of photoblotted and immunoprobed TurboGFP. On the left, a false-color micrograph of photoblotted TurboGFP protein after electrophoretic separation, with a corresponding intensity profile. On the right, a false-color micrograph of the TurboGFP immunoblot, with corresponding intensity profile. Arrowheads mark the position of each protein peak. Scale bars are 200 µm, unless specified.

us to link genome, transcriptome and proteome in challenging cell types with low availability, such as rare cell populations (e.g., circulating tumor cells, or CTCs) or stem cells[28], or other cells that cannot be expanded by culture (e.g., cells from biopsies)[18]. Measurements with single- or few-cell resolution are also essential to studying cell-to-cell heterogeneity and distinguishing different population distributions (e.g., bimodal vs. normally-distributed expression) which may have the same population mean expression level[29]. However, the specificity of the protein measurement in such assays typically relies on antibody probes alone, which are subject to nonspecific cross-reactivity and cannot detect isoforms without isoform-specific antibody probes. Thus, selective detection of specific protein isoforms is problematic when isoform-specific antibody probes are not available[30]. While Western blotting adds specificity by separating protein isoforms by mass prior to antibody-based detection, conventional Western blotting requires 10,000s of cells[28]. As a result, identifying different proteoforms arising from modifications to DNA or mRNA at the single- or few-cell scale remains extremely challenging. Recently introduced multimodal assays that perform multimodal protein isoform and nucleic acid detection were specifically designed for murine embryos, which are ~100 times larger in volume than somatic cells, and only demonstrated detection of mRNA and not DNA[31,32].

Here, we perform same-cell DNA, mRNA and protein isoform immunoblotting measurements (triBlot) on low starting cell numbers (i.e. 1 to 100s of cells); a clinically relevant range that includes single CTCs and CTC clusters[33], as well as cells recovered from needle biopsies (100s)[34,35]. Our technique first fractionates cells into nuclear and cytoplasmic compartments. The cytoplasmic fraction undergoes polyacrylamide gel

electrophoresis (PAGE), while the nuclei are excised from the triBlot device and analysed for mRNA and/or DNA. We measure expression of protein isoforms from the cytoplasmic fraction of 1-100s cells, while achieving same-sample analysis of DNA and of mRNA retained in the nuclei where nuclear mRNA has been demonstrated to generally correlate well with whole-cell mRNA expression[36–38].

Results and discussion

Design of same-cell protein and nucleic acid assay for low starting cell numbers

In order to perform multimodal measurements on the same mammalian cells, we developed an assay that integrates (i) electrophoretic separation of cytoplasmic proteins and (ii) extraction of nucleic acids from the nuclei. To do so, we designed the triBlot device, consisting of a 200 μm-thick polyacrylamide (PA) gel covalently bound to the treated surface of a flexible polyester film (Gelbond™ PAG Film). The PA layer is in turn patterned with an array of microwells (200 μm in diameter)[32].

Our assay begins with settling cells into the microwells of the triBlot device (Fig. 1a). Cells can be passively settled into microwells by gravity[39], or actively sampled using a micromanipulator[40,41] or a mouth-pipette assembly[31]. In terms of sample requirements, one microwell can hold from one single cell to ~200 cells. Given that the triBlot device has 45 microwells, 45 separate samples can be analyzed simultaneously, each sample ranging from a single cell to ~200 cells. Treatment of cells with fractionation lysis buffer[31,42] for 1 minute achieves *in situ* lysis of the cytoplasmic fraction of cells (Fig. 1a). An electric field is then applied for 2 to 3 minutes to (i) inject solubilized proteins through the microwell wall and into the PA gel layer and (ii) achieve fractionation PAGE (fPAGE), which separates cytoplasmic proteins by molecular mass along the *separation lane*, or region abutting the microwell. Proteins are then photo-blotted, or immobilized to the PA layer by 45-second long UV-light activation of benzophenone moieties incorporated in the PA gel matrix. After cytoplasmic fPAGE, the nuclei remain intact in the microwells. The polymer substrate of the triBlot device allows us to laser-excise areas of the gel, or *gel pallets*, containing the microwells with the fractionated nuclei. Nuclei-laden gel pallets are then placed into reaction vessels (Eppendorf tubes) in order to perform extraction and off-chip analysis of either DNA or mRNA. The remaining triBlot device is then immunoprobed for proteins with fluorescently-labelled antibody probes, yielding protein immunoblots from the original settled cells.

Questions surrounding rare-cell types, such as CTCs and CTC clusters, may require simultaneous analysis of a wide range of cell numbers. To determine the dynamic range of our assay, we utilized U251 human glioblastoma cells engineered to express the fluorescent protein TurboGFP in the cytoplasm, but not the nucleus)[42]. Expression of fluorescent TurboGFP is a useful protein model for visualizing cell lysis, injection, fPAGE, and photo-blotting. We first settled TurboGFP-U251 cells stained with nuclear Hoechst dye into microwells (Fig. 1b). After fractionation lysis, fPAGE and photocapture, we observed a TurboGFP band in the separation lane along with absence of TurboGFP fluorescence in the microwell, suggesting complete lysis and injection of the cytoplasmic proteins into the PA gel had been achieved (Fig. 1b).

Next, to maintain the integrity of the nuclei we place the gel device in nuclei wash buffer. We then excised gel pallets containing the microwells (Fig. 1c). Fluorescence imaging of the Hoechst-stained nuclei confirmed the presence of the nuclei in the microwells (Fig. 1c). The remaining gel device was imaged for native TurboGFP signal and then incubated with primary antibody probes against TurboGFP followed by AlexaFluor555-conjugated secondary antibody probes and imaged for resulting TurboGFP immunoblots (Fig. 1d). The detection of two bands in both the photo-blotted and the immunoprobed protein bands (Fig. 1d) indicates the ability to discern protein isoforms using the same antibody probe. Isoforms of GFP, which are estimated to differ by less than 1 kDa in molecular mass, have been attributed to differential C-terminal cleavage by non-specific proteases during bacterial expression of recombinant proteins[43].

Extraction of gel pallets enables quantification of DNA from a single nucleus

We next sought to scrutinize the viability of nucleic acid analysis after gel pallet retrieval and determine detection limits. To do so, we performed amplification of the TurboGFP gene by polymerase chain reaction (PCR) from gel pallets containing a single nucleus (Fig. 2a). We designed microwells to isolate single TurboGFP-expressing U251 cells (32 μm in diameter, 40 μm in height). After fPAGE of the cytoplasmic fraction, single nuclei retained in the microwells were excised into gel pallets. To verify retention of each nucleus, we used epifluorescence microscopy to inspect gel pallets for the Hoechst-stained nuclei. Gel pallets were then placed into separate reaction vessels

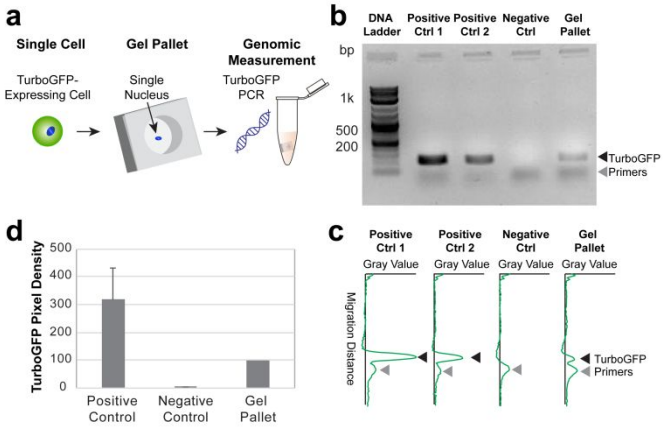

Figure 2 PCR amplification of TurboGFP DNA from a gel pallet containing a single TurboGFP-expressing U251 cell nucleus. (a) Schematic of gel pallets analyzed for TurboGFP DNA. (b) Agarose gel electrophoresis of DNA amplified for the TurboGFP gene by PCR from samples including: positive controls (10 μg DNA extracted from TurboGFP-U251 lysate), negative controls (no DNA) and gel pallet containing one TurboGFP-U251 nucleus. (c) Gray value intensity profiles for agarose gel lanes corresponding to positive controls, negative control and gel pallet containing a single TurboGFP-U251 nucleus. (d) Bar

plots of densitometric quantitation of TurboGFP bands in agarose gel electrophoresis. Error bars indicate standard deviation for n = 3 replicates.

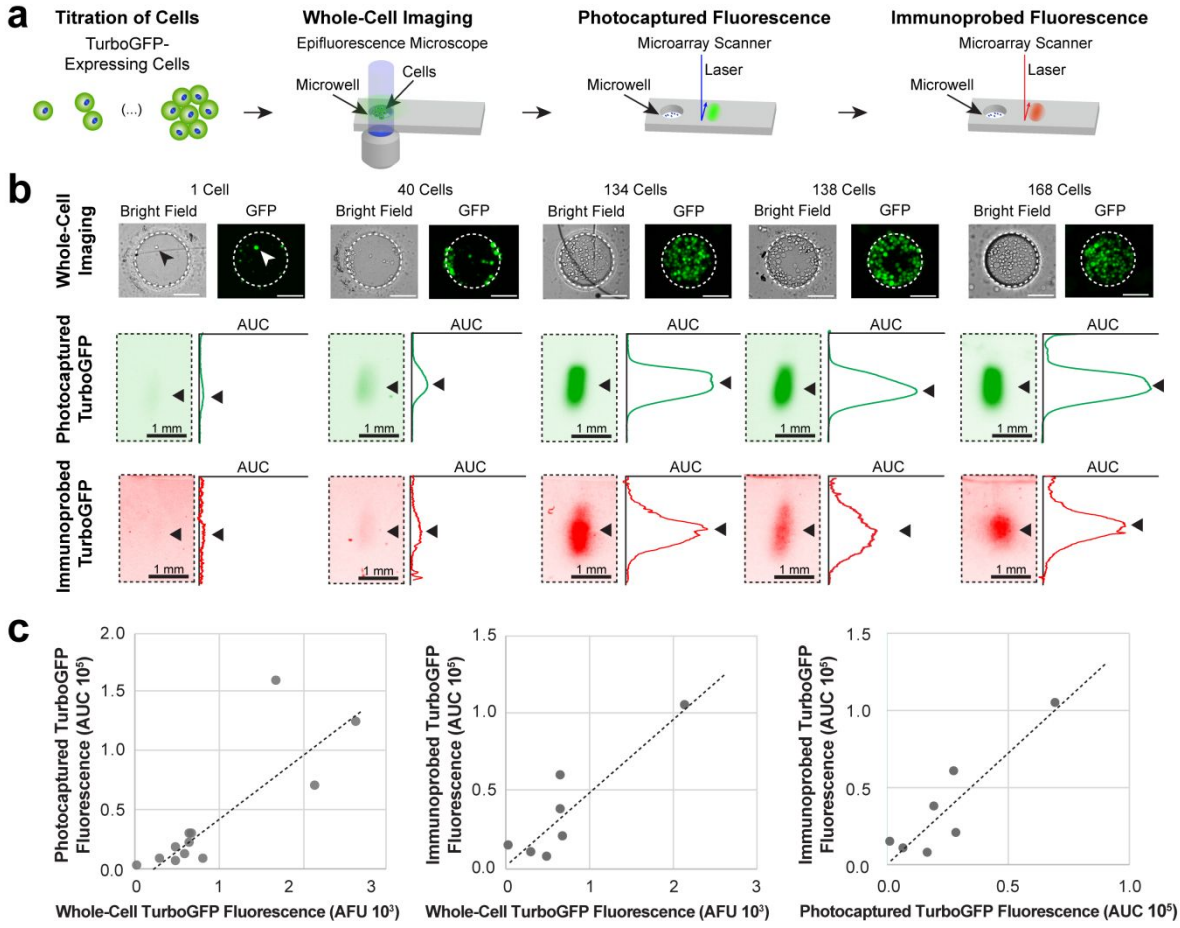

Figure 3 Photo-blotted and immunoprobed protein quantitation correlates with protein expression measured prior to lysis. (a) Schematic of experiment for quantifying TurboGFP protein at different stages of the same-cell nucleic acid and protein isoform measurement assay. (b) Brightfield and false color fluorescence micrographs of TurboGFP-expressing U251 cells settled into microwells. Cells were manually counted in ImageJ using overlay brightfield and GFP micrographs. Corresponding false color fluorescence micrographs of TurboGFP immunoblots imaged after photo-blotting and immunoprobing. Fluorescence intensity profiles are shown to the right of immunoblots. Black arrows mark the position of protein peaks. (c) Bivariate plots of whole-cell TurboGFP fluorescence prior to lysis, photo-blotted TurboGFP fluorescence (AUC) and immunoprobed TurboGFP fluorescence (AUC). Whole-cell TurboGFP fluorescence shows strong positive correlation with both photo-blotted and immunoprobed TurboGFP fluorescence (Pearson correlation, $\rho = 0.839$ and 0.902, for N = 9 and 7 microwells, respectively). Likewise, photo-blotted and immunoprobed TurboGFP fluorescence show a strong positive correlation (Pearson correlation, $\rho = 0.909$, N = 7 microwells).

(centrifuge tubes) for PCR amplification of the TurboGFP gene. PCR products were analysed on an agarose gel, revealing successful amplification of the TurboGFP from the gel pallet (Fig. 2b, 2c). The presence of a PCR product of the same length as the positive control indicates amplification of the TurboGFP gene from the gel pallet sample, validating viability of DNA extraction from nuclei in gel pallets (Fig. 2b, 2c). Densitometry analysis of the PCR product enables semi-quantitative analysis of the DNA present in the gel pallets (Fig. 2d). Results indicate DNA can be retrieved from gel pallets from starting samples containing as few as a single nucleus per gel pallet.

Photo-blotted and immunoblotted protein fluorescence signal correlates with protein expression prior to lysis

We next evaluated the performance of our assay in measuring protein targets, namely, whether protein measured after lysis, fPAGE and immunoblotting accurately measures protein abundance prior to lysis. We used the TurboGFP protein in TurboGFP-expressing U251 cells as a measure of protein abundance. We first loaded an increasing number of cells into microwells of a triBlot device, from a single cell to ~200 cells (Fig. 3a). We imaged the TurboGFP-U251 cells settled into microwells for TurboGFP fluorescence prior to lysis and computed whole-cell fluorescence intensity by area-under-the-curve analysis (AUC). We then ran fPAGE and scanned the triBlot device for photo-blotted native TurboGFP fluorescence. Finally, we immunoprobed the triBlot devices with primary antibody probes against TurboGFP (rabbit-anti-TurboGFP), followed by fluorophore-conjugated secondary antibody probes (AlexaFluor555 donkey-anti-rabbit), and imaged the devices for immunoprobed TurboGFP signal. To quantify the photo-blotted and immunoprobed protein peaks, we performed Gaussian curve fitting on the protein peak intensity profiles and used the Gaussian fit parameters (peak center and

σ) to calculate the AUC for a peak width of 4σ. Quality control metrics were defined as signal-to-noise ratio (SNR) greater than 3 and a Gaussian fit $R^2 > 0.6$.

When comparing (i) whole-cell TurboGFP prior to lysis, (ii) native signal from the photo-blotted TurboGFP and (iii) immunoprobed signal from fluorophore-conjugated antibody probes against TurboGFP (Fig. 3a), we found that whole-cell TurboGFP fluorescence demonstrated a positive linear association with signal quantified from both photo-blotted TurboGFP fluorescence and immunoblotted TurboGFP fluorescence (Pearson correlation, $\rho = 0.839$ and 0.902, for N = 9 and 7 microwells, respectively). Photo-blotted and immunoprobed TurboGFP fluorescence also show a strong positive correlation (Pearson correlation, $\rho = 0.909$, N = 7 microwells, Fig. 3b). These results suggest that endpoint immunoblots accurately estimate protein abundance in starting, intact cells. These results further suggest that endpoint immunoblotting can accurately quantify endogenous protein targets (not tagged with fluorescent labels) for which pre-lysis quantification is impossible. Finally, the limit of detection (LOD) for proteins has been experimentally determined to be 27,000 copies[44], corresponding to single-cell levels of a median-expressed protein[45]. As with any immunoassay, the LOD is dependent on antibody probe affinity for protein target epitope.

TurboGFP mRNA correlates with TurboGFP protein fluorescence measured prior to lysis, after fPAGE and after immunoprobing

We next examined whether mRNA collected from gel pallets correlates with protein expression. First, we examined if mRNA extracted from gel pallets containing single nuclei could be amplified. We used a single-cell droplet printer (cellenONE) to deposit single TurboGFP-expressing U251 cells into microwells of a triBlot device. After performing fPAGE with a 25 sec lysis time, we excised gel pallets containing single nuclei and processed them for mRNA analysis (Fig. 4a). We extracted and amplified mRNA from gel pallets and analysed amplified cDNA for TurboGFP by RT-qPCR (Fig. 4b). To ensure the triBlot assay can support a single-cell LOD for mRNA, we used a kit that has been validated to detect transcripts from single cells by the manufacturer (Zymo). All samples prepared from gel pallets show higher expression (i.e. lower C_T values) than all negative controls (high or absent C_T values), including a sample containing TurboGFP-expressing U251 cDNA where the reverse transcriptase (RT) enzyme was left out (-RT), an RT mix only sample, a PreAmplification only sample and a sample containing primer but no cDNA sample to test for background primer dimer amplification (Fig. 4b, 4c). Positive controls were cDNA from TurboGFP-U251 cell lysate (Pos Ctrl 1) and cDNA from a gel pallet containing multiple U251 nuclei (Pos Ctrl 2). Positive controls amplified either before or at similar CT values as samples from gel pallets containing a single TurboGFP-expressing U251 cell (Fig. 4b, 4c). Companion TurboGFP immunoblots showed protein peaks that passed the quality control metrics of SNR > 3 and Gaussian fit $R^2 > 0.6$ (Fig. 4d).

Finally, to examine correlations between mRNA and protein expression, we used passive gravity settling to load increasing numbers of cells into the microwells of a triBlot device. We loaded from 6 cells per microwell to 201 cells per microwell. After fPAGE and excision of the triBlot device into gel pallets, gel pallets were placed into separate reaction vessels containing DNA/RNA Shield™ solution (Zymo) to extract mRNA from retained nuclei (Fig. 5a). While devices were immunoprobed with antibody probes against TurboGFP, isolated mRNA was first reverse transcribed and subsequent cDNA was analyzed for TurboGFP expression using semi-quantitative real-time PCR analysis (semi-RT-qPCR). Amplified cDNA was analyzed by agarose gel electrophoresis and bands were quantified by densitometry (Fig. 5b). We observed an 85% yield for successful sample amplification, where 12 out of 15 samples had a detectable band at the correct TurboGFP amplicon length (Fig. 5b, lanes 2-7, 9 and 11-15). To determine a failed amplification, we used the presence of a primer band and absence of a TurboGFP band (Fig. 5b, lanes 8 and 10).

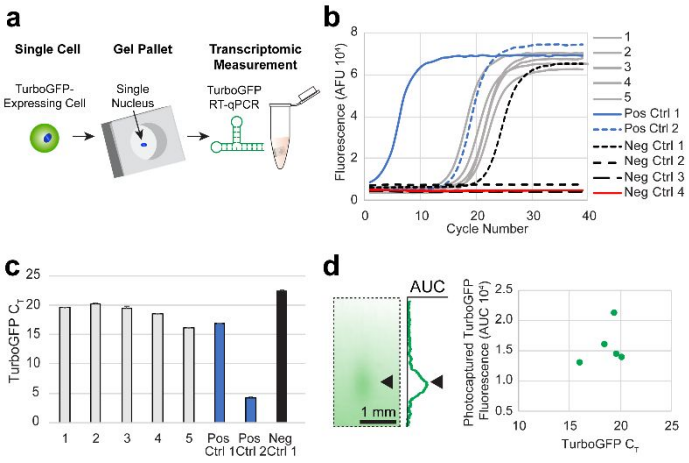

Figure 4 RT-qPCR amplification of mRNA from gel pallet containing single TurboGFP-expressing U251 cell nucleus. (a) Schematic of gel pallets analyzed for TurboGFP mRNA. (b) RT-qPCR Amplification curves for TurboGFP from gel pallets containing a single nucleus (Samples 1-5), positive controls (Pos Ctrl 1: gel pallet containing multiple TurboGFP-U251 nuclei and Pos Ctrl2: cDNA amplified from TurboGFP-U251 lysate) and negative controls (Neg Ctrl 1: cDNA from lysate without RT mix, Neg Ctrl 2: RT mix only, Neg Ctrl 3: PreAmplification mix only, Neg Ctrl 4: primers only with no cDNA to test for background from primer dimer amplification). (c) Bar graph of TurboGFP C_T values for all samples shown in panel (b) that amplified. Error bars indicate standard deviation for n = 3 replicates. (d) On left, false color fluorescence micrograph showing TurboGFP band from a single U251 cell with accompanying intensity profile to the right. Arrowheads mark the position of protein peak. On the right, bivariate plot of photocaptured TurboGFP fluorescence (AUC) and TurboGFP CT values for samples containing a single U251 nucleus (n = 5 gel pallets containing a single U251 nucleus).

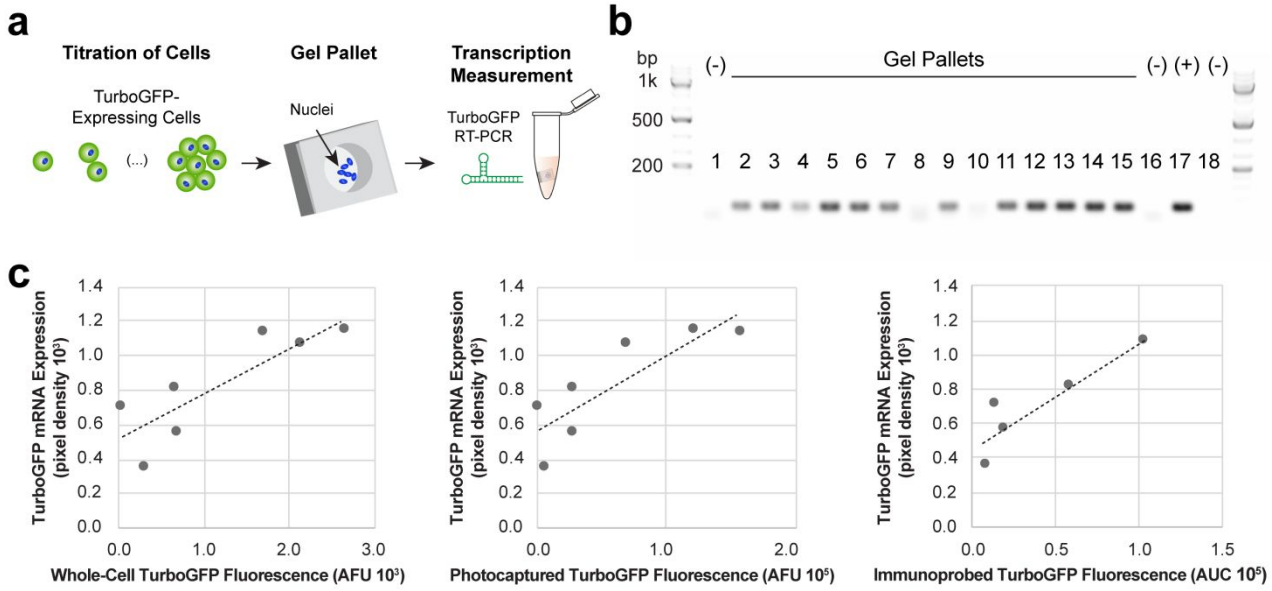

Figure 5 semi-RT-qPCR amplification of TurboGFP mRNA from gel pallets correlates with same-cell protein expression measurement. (a) Schematic of analysis of gel pallets for TurboGFP mRNA. (b) Agarose gel electrophoresis of cDNA amplicons representing gel pallets with increasing number of cells (lanes 2-*15).* Negative controls include lanes 1 (no cells), lane 16 (-RT) and lane 18 (water). Positive control lane 17 containing TurboGFP plasmid (1ng) was positive. DNA ladder used was Thermo 1KB+ DNA Ladder. (c) Semi quantitative mRNA TurboGFP levels, measured from densitometry plots of *c*DNA agarose gel, demonstrate strong linear correlation with all protein measurements; whole-cell, photo-blotted and immunoprobed TurboGFP fluorescence (Pearson correlation, ρ = 0.849, 0.843 and 0.907, for N = 7, 7 and 5 microwells, respectively).

Results show that whole-cell fluorescence and photo-blotted protein signal are significantly correlated with mRNA levels (Pearson correlation, ρ = 0.849 and 0.843, N = 7 microwells, for whole-cell TurboGFP fluorescence and photo-blotted TurboGFP, respectively, Fig. 5c. Failed PCR amplification samples or samples with protein peaks that did not pass QC metrics of SNR > 3 and R^2 > 0.6 were not considered). TurboGFP mRNA levels also show a strong positive association with immunoprobed TurboGFP signal (Pearson correlation, N = 5 microwells, ρ = 0.907, Fig. 5c). These results validate the integrity of mRNA recovered from nuclei-laden gel pallets, and demonstrate that transcription levels can be quantified from same-cell mRNA and immunoblotting assay.

Experimental

Chemical reagents. Tetramethylethylenediamine (TEMED, T9281), ammonium persulfate (APS, A3678), β-mercaptoethanol (M3148), 30%T/2.7%C acrylamide/bis-acrylamide (37.5:1) (A3699), bovine serum albumin (BSA, A9418), Tyrode's solution (T1788), trypsin 10X (59427C), digitonin (D141), sucrose (S0389-500G), magnesium chloride (M8266) and HEPES (90909C) were purchased from Sigma-Aldrich. Triton X-100 (BP-151), phosphate-buffered saline (PBS, pH 7.4, 10010023), SYBR Gold (S11494), agarose (BP-1356-500) were purchased from Thermo Fisher Scientific. Premixed 10X tris-glycine electrophoresis buffer (25 mM Tris, pH 8.3; 192 mM glycine; 0.1% SDS) was purchased from Bio-Rad. Tris buffered saline with Tween-20 (TBST) was prepared from 20X TBST (sc-24953, Santa Cruz Biotechnology, Dallas, TX). Deionized water (18.2 MΩ) was obtained using an Ultrapure water system from Millipore. N-[3-[(3-Benzoylphenyl)formamido]propyl] methacrylamide (BPMAC) was custom synthesized by Pharm-Agra Laboratories (Brevard, NC). GelSlick™ (50640) and Lonza™ GelBond™ PAG Film for Acrylamide Gels (BMA54746) was purchased from Lonza. Taq PCR kit (E5000S), proteinase K (P8107S) were purchased from New England Biosciences.

Buffer compositions. Fractionation lysis buffer: 0.125 mg/mL digitonin, 1% v/v Triton X-100 and 0.5 X Tris-glycine. Nuclei wash buffer: 320 mM sucrose, 5 mM $MgCl_2$, 10 mM HEPES.

Cell culture. U251 human glioblastoma cells were obtained from the UC Berkeley Tissue Culture Facility via the American Type Culture Collection and stably transduced with TurboGFP via lentiviral infection (multiplicity of infection 10). Cells were cultured in high-glucose Dulbecco's modified eagle medium (DMEM) (11965, Life Technologies) supplemented with 1× MEM nonessential amino acids (11140050, Life Technologies), 100 U mL^{-1} penicillin-streptomycin (15140-122, Life Technologies), 1 mM sodium pyruvate (11360-070), and 10% fetal bovine serum (JR Scientific, Woodland) in an incubator at 37 °C with humidified 5% CO_2 air.

Device fabrication. SU-8 wafers, fabricated by photolithography as previously reported[46], were used as molds to cast triBlot devices. SU-8 posts on wafers, which later translate into microwells in the PA gel, were 200 μm in diameter and 200 μm in height[32]. A modified wafer generating microwells 100 μm in diameter and 110 μm in height was used for triBlot assays of single cells. Briefly, PA precursor solution including acrylamide/bis-acrylamide (10%T) and 3 mM BPMAC was

degassed with sonication for 9 min. 0.08% APS and 0.08% TEMED were added to precursor solution and solution was pipetted between the SU-8 wafer (rendered hydrophobic with Gel Slick™ solution) and a GelBond™ Film cut to the size of a standard glass microscope slide (25 mm x 75 mm). After chemical polymerization (20 min) the triBlot devices (thin PA gel layer covalently grafted onto the GelBond™ surface) were lifted from wafer, rinsed with deionized water and stored in hydrated (DI water) at 4°C until use.

Fractionation PAGE of 1-100s U251-TurboGFP cells. TurboGFP-expressing U251 cells were harvested from tissue culture plates by incubation in trypsin/EDTA (15090046, Thermo) at 37°C for 5 min. Trypsin was inactivated by addition of FBS and cells were pelleted by centrifugation at 100 rcf. After removal of supernatant, cells were resuspended in PBS at $1x10^6$ cells / mL. For triBlot assays of single cells, cells were settled using the CellenONE single-cell dispenser as described below. For all other experiments, cells were gravity settled as follows: 1 mL of this cell suspension was pipetted over the triBlot device and cells were allowed to settle into microwells for 10 min. Excess cells not settled into microwells were then washed off the PA gel surface with PBS and microwells were imaged by bright field and fluorescence microscopy (Olympus IX71 microscope, Lumen Dynamics X-cite fluorescence illumination source coupled to a liquid light guide (Lumatec, 805-00038), 10X (0.3 NA) objective (Olympus UPLANFL10X), DAPI (Omega XF02-2) and GFP (Chroma 49011 ET) filter cubes, and an Andor iXon+ EMCCD camera (DU-885K-C00-#VP)) to collect data on number of cells per microwell and TurboGFP expression. The device was placed into an electrophoresis (EP) chamber, and fractionation lysis buffer (RT, 12 mL) poured over the gel and incubated for 1 min. fPAGE was performed at 40 V/cm for 2-3 min (depending on the assay). Immobilization of proteins by photocapture was carried out by illumination with UV light source (100% power, 45 s, Lightningcure LC5, Hamamatsu). Gels were quickly placed in ice-cold nuclei wash buffer, and buffer was exchanged three times before proceeding to laser excision. Nuclei remaining in wells can be laser-excised, while proteins immobilized on membrane can be probed with fluorescently-labeled antibody probes.

Laser excision of triBlot device into gel pallets. Gel pallets were excised from the device as previously described[32]. Briefly, the PA gel was kept hydrated at all times with nuclei wash buffer and kept over ice between excision events. A CO_2 laser cutter (HL40-5G-110, Full Spectrum Laser) was used to excise gel pallets from triBlot devices. The device was placed with the PA gel face down onto a clear acrylic sheet (McMaster-Carr) engraved with a 5 x 5 mm grid. Using a bright field microscope, microwells were aligned to be horizontally centered above a grid square and approximately 1 mm away from the top edge of each square. The laser was aligned over the left corner of a grid square and programmed to cut at 10% power, 20 speed and 1 pass.

Antibody probes. Rabbit anti-TurboGFP (PA5-22688), AlexaFluor647-conjugated donkey anti-rabbit secondary (A31572) and AlexaFluor555-conjugated donkey anti-rabbit (A-31572) were purchased from Thermo Fisher Scientific.

Immunoprobing and fluorescence imaging of photo-blotted protein and immunoblots. After laser excision, devices were washed in deionized water and a 25 mm x 75 mm coverslip was placed over the hydrated PA gel. Devices were imaged in a microarray scanner (Genepix 4300A, Molecular Devices) for photo-blotted TurboGFP protein with the cover slip facing down. Devices were then washed in 1X TBST for at least 1 hr before probing with antibody probes. Primary antibody probes were incubated at 1:10 dilution (80 μL/gel, in 2% BSA in 1X TBST), while fluorophore-conjugated secondary antibody probes were incubated at 1:20 dilution (80 μL/gel, in 2% BSA in TBST). Devices were scanned again for fluorescence immunoblot signal.

Protein band image analysis. Protein expression was quantified by area-under-the-curve analysis (AUC) of immunoblots as previously described. Briefly, custom MATLAB scripts were used to fit Gaussian curves to protein band intensity profiles. Gaussian fit parameters of peak location and σ were used to calculate the AUC for a peak width of 4σ. Protein bands passed quality control metrics if signal-to-noise ratio (SNR) was higher than 3 and the Gaussian fit R^2 was equal to or greater than 0.6.

Single-gel pallet PCR. After laser excision, gel pallets were placed into a 0.5 mL PCR tube containing 2.5 μL Molecular Grade water, 1 μL SDS (17 μM to final concentration of 3.4 μM) and 1.5 μL proteinase K. Tubes were incubated at 45°C for 15 min followed by proteinase K inactivation by incubation at 95°C for 20 min. Next, the following were added to each tube: 2.5 μL TurboGFP primers (at 500 nM, purchased from Integrated DNA Technologies, sequences: (5'TGA TGG GCT ACG GCT TCT A, 5'GTG TTG CTG TGA TCC TCC TC), 1 μL dNTPs (at 200 μM, Taq PCR Kit), 0.25 μL Taq polymerase (Taq PCR Kit), 5 μL of Standard Taq Reaction Buffer 10X (Taq PCR Kit) and water up to 50 μL. Template DNA (~200 ng/μL) extracted TurboGFP-U251 lysate was added to positive control tubes. Negative controls did not contain DNA or gel pallets. For amplification of the TurboGFP gene, the following cycle steps were programmed using a thermal cycler (PTC-100™, MJ Research Inc): the first stage at 95°C for 10 min, the second stage (annealing at 51°C for 30 s, extension at 72°C for 30 s, denaturation at 95°C for 30 s) for 45 amplification cycles, and a final stage at 72°C for 10 min. PCR products were analyzed on a 1% agarose gel by EP. SYBR Gold was used at 1X to stain agarose gels and a ChemiDoc™ XRS+Gel Imaging System (Bio-Rad) was used to image the DNA bands. Gels were analyzed by densitometry using ImageJ[47].

Single-cell deposition with cellenONE system

Single cells were deposited into 100 μm diameter and 110 μm deep microwells in the triBlot device with the cellenONE X1 Droplet Printer (Scienion, Berlin, Germany) and a cellenONE PDC M Piezo Dispensing Capillary (PDC-20-CM). TurboGFP-U251

cells were diluted to a concentration of 300,000 cells/mL in PBS. The triBlot PA gel was briefly dried with a nitrogen stream before droplet deposition. Crosshair-shaped fiducial markers on the gel were used in conjunction with the "Find Target Reference Points" software function to align droplets to microwells. The target plate temperature was set to 4°C to prevent the evaporation of deposited droplets. Single-cell occupancy in droplets was verified by imaging the interior of the PDC prior to droplet deposition. The PDC M deposits droplets of 350 – 400 pL in volume. After deposition, the single cells were immediately fractionally lysed.

Single-gel pallet quantitative reverse transcription Polymerase chain reaction (RT-qPCR). Once excised, each gel pallet was transferred to one centrifuge tube, immediately followed by the addition of 20 µL of DNA/RNA Shield™ (R1100, Zymo). Sample were stored in -80ºC until RNA preparation. RNA and DNA were isolated following the manufacturer's protocol. Nucleic acids were eluted in 8 µL of water. Alternate mRNA and DNA isolation can be performed with Direct-zol™ RNA Miniprep Plus (Cat. R2070S, LOT: ZRC202000), RNA Clean & Concentrator™-5 Cat R1015S (10 preps), LOT: ZRC200969). All 8 µL of RNA sample was used for cDNA synthesis. Reverse transcription of mRNA to cDNA was accomplished with SuperScript IV First Strand Synthesis System (18091050, Thermo Fisher) as per manufacturer instructions. Pre-amplification was done on the resulting 20-µl cDNA sample using the Perfecta PreAmp SuperMix (95146 QuantaBio) as per the manufacturer's instructions, and using the 14 cycle option and a subsequent 20x dilution into nuclease free water (am9937, Fisher). All RT-qPCR reactions were performed using SSO Universal SYBR Green SuperMix, as per manufacturer instructions (1725275, BioRad). Primer sequences used were TurboGFP (5'TGA TGG GCT ACG GCT TCT A, 5'GTG TTG CTG TGA TCC TCC TC). All RT-qPCR analyses were performed on the StepOnePlus Real Time PCR system (437660, Thermo).

Conclusions

Assessing whether specific modifications at the nucleic acid level drive important mechanisms in disease progression requires measuring all molecular types involved, including proteins, DNA and mRNA. Here we design an assay for simultaneous measurement of protein isoforms and nucleic acids from low starting numbers of mammalian cells. We demonstrate that signal from immunoprobed protein correlates strongly with protein expression prior to lysis in TurboGFP-expressing cells. We also measure both mRNA and DNA from retrieved nuclei, with positive amplification of TurboGFP gene and TurboGFP transcripts, demonstrating our ability to recover, isolate and amplify nucleic acids from gel pallets. The cell number range over which we performed these measurements (from 1 to 100s of cells) includes the cell numbers relevant to tumor samples, including cells obtained from fine needle aspirates and CTC clusters.

Given the prevalence of protein isoforms across a wide range of diseases, tools that measure both nucleic acids and intracellular protein isoforms from the same cells are necessary to (i) reveal the mechanisms by which the events at the nucleic acid level (including SNPs, alternative splicing or PTMs) regulate the production of pathogenic proteoforms, and (ii) identify new disease-specific biomarkers for early detection, diagnosis, and therapy.

Moreover, as more efficient gene editing tools continue to emerge, strict evaluation of how both on-target and off-target edits affect the transcriptional and protein expression landscapes will become critical for safely translating these gene editing tools into clinical applications[48,49]. Same-cell multimodal tools such as the one presented here will be instrumental in unequivocally linking modifications in protein expression profiles to on-target and off-target editing events.

Conflicts of interest

Authors are inventors on pending patents relating to simultaneous protein and mRNA measurements.

Acknowledgements

The authors acknowledge members and alumni of the Herr Lab for helpful discussions. Partial infrastructure support was provided by the QB3 Biomolecular Nanofabrication Center. This research was performed under a National Institutes of Health Training Grant awarded to the UCB/USCF Graduate Program in Bioengineering (5T32GM008155-29 to E.R.C. and A. Geldert .), a California Institute for Regenerative Medicine Predoctoral Fellowship (E.R.C.), an Obra Social "la Caixa" Fellowship (E.R.C.), a University of California, Berkeley Siebel Scholarship (E.R.C. and A. Gopal), a National Defense Science and Engineering Graduate Fellowship (to A. Geldert.), National Science Foundation Graduate Student Fellowship Program (DGE 1752814 to A.E.G.M), a National Science Foundation CAREER Award (CBET-1056035 to A.E.H.), National Institutes of Health grants (1R01CA203018 to A.E.H.; R01GM114414, R01CA139067, 2R01CA139067, 1R21HD088885 and R21HD088885 to L.H.), a Howard Hughes Medical Institute (HHMI) Faculty Scholar Award (L.H.), a Bakar Fellow award at UC Berkeley (L.H.), a research scholar award from the American Cancer Society (L.H.), and an K99/R00 Pathway to Independence Fellowship from the National Institutes of Health (HD096108 to A.J.M .) and a Fellow of the Siebel Stem Cell Institute (to A.J.M).

Notes and references

1. Barrett, C. L. *et al.* Systematic transcriptome analysis reveals tumor-specific isoforms for ovarian cancer diagnosis and therapy. *Proc. Natl. Acad. Sci. U. S. A.* **112**, E3050–E3057 (2015).
2. Frankiw, L., Baltimore, D. & Li, G. Alternative mRNA splicing in cancer immunotherapy. *Nat. Rev. Immunol.* **19**, 675–687 (2019).
3. Martinez, B. I. & Stabenfeldt, S. E. Current trends in

biomarker discovery and analysis tools for traumatic brain injury. *J. Biol. Eng.* **13**, 1–12 (2019).
4. Ward, M. & Schofield, E. L. Biomarkers for brain disorders. *Therapy* **7**, 321–336 (2010).
5. Wei, J., Zaika, E. & Zaika, A. P53 family: Role of protein isoforms in human cancer. *J. Nucleic Acids* **2012**, (2012).
6. Bruikman, C. S., Zhang, H., Kemper, A. M., Van Gils, J. M. & Majerciak, V. Netrin Family: Role for Protein Isoforms in Cancer. *J. Nucleic Acids* **2019**, (2019).
7. Climente-González, H., Porta-Pardo, E., Godzik, A. & Eyras, E. The Functional Impact of Alternative Splicing in Cancer. *Cell Rep.* **20**, 2215–2226 (2017).
8. Lorentzian, A., Uzozie, A. & Lange, P. F. Origins and clinical relevance of proteoforms in pediatric malignancies. *Expert Rev. Proteomics* **16**, 185–200 (2019).
9. Jovanov-Milošević, N. *et al.* Human fetal tau protein isoform: Possibilities for Alzheimer's disease treatment. *Int. J. Biochem. Cell Biol.* **44**, 1290–1294 (2012).
10. Stuart, T. & Satija, R. Integrative single-cell analysis. *Nat. Rev. Genet.* **20**, 257–272 (2019).
11. Ståhlberg, A., Thomsen, C., Ruff, D. & Åman, P. Quantitative PCR analysis of DNA, RNAs, and proteins in the same single cell. *Clin. Chem.* **58**, 1682–1691 (2012).
12. Ruggles, K. V. *et al.* Methods, tools and current perspectives in proteogenomics. *Mol. Cell. Proteomics* **16**, 959–981 (2017).
13. Qui, S. *et al.* Analysis of plasma HER2 copy number in cell-free DNA of breast cancer patients: a comparison with HER2 extracellular domain protein level in serum. *Breast Cancer* (2021). doi:10.1007/s12282-020-01212-x
14. Zhao, Y. *et al.* Nanoscale imaging of clinical specimens using pathology-optimized expansion microscopy. *Nat. Biotechnol.* 757–764 (2017).
15. Louie, R. H. Y. & Luciani, F. Recent advances in single-cell multimodal analysis to study immune cells. *Immunol. Cell Biol.* 157–167 (2021). doi:10.1111/imcb.12432
16. Nathan, A., Baglaenko, Y., Fonseka, C. Y., Beynor, J. I. & Raychaudhuri, S. Multimodal single-cell approaches shed light on T cell heterogeneity. *Curr. Opin. Immunol.* **61**, 17–25 (2019).
17. Stoeckius, M. *et al.* Simultaneous epitope and transcriptome measurement in single cells. *Nat. Methods* **14**, 865–868 (2017).
18. Macaulay, I. C., Ponting, C. P. & Voet, T. Single-cell multiomics: multiple measurements from single cells. *Trends Genet.* **33**, 155–168 (2017).
19. Gawad, C., Koh, W. & Quake, S. R. Single-cell genome sequencing: Current state of the science. *Nat. Rev. Genet.* **17**, 175–188 (2016).
20. Schwartzman, O. & Tanay, A. Single-cell epigenomics: Techniques and emerging applications. *Nat. Rev. Genet.* **16**, 716–726 (2015).
21. Wu, M. & Singh, A. K. Single-Cell Protein Analysis. *Curr. Opin. Biotechnol.* **23**, 83–88 (2012).
22. Stegle, O., Teichmann, S. A. & Marioni, J. C. Computational and analytical challenges in single-cell transcriptomics. *Nat. Rev. Genet.* **16**, 133–145 (2015).
23. Xue, M. *et al.* Chemical methods for the simultaneous quantitation of metabolites and proteins from single cells. *J. Am. Chem. Soc.* **137**, 4066–4069 (2015).
24. Peterson, V. M. *et al.* Multiplexed quantification of proteins and transcripts in single cells. *Nat. Biotechnol.* **35**, 936–939 (2017).
25. Frei, A. *et al.* Highly multiplexed simultaneous detection of RNAs and proteins in single cells. *Nat Methods* **3**, (2016).
26. Albayrak, C. *et al.* Digital Quantification of Proteins and mRNA in Single Mammalian Cells. *Mol. Cell* **61**, 914–924 (2016).
27. Kawai, T. *et al.* Ultrasensitive Single Cell Metabolomics by Capillary Electrophoresis–Mass Spectrometry with a Thin-Walled Tapered Emitter and Large-Volume Dual Sample Preconcentration. *Anal. Chem.* **91**, 10564–10572 (2019).
28. Cai, X., Zheng, Y. & Speck, N. A. A western blotting protocol for small numbers of hematopoietic stem cells. *J. Vis. Exp.* **2018**, 6–9 (2018).
29. Altschuler, S. J. & Wu, L. F. Cellular Heterogeneity: Do Differences Make a Difference? *Cell* **141**, 559–563 (2010).
30. Trenchevska, O., Nelson, R. W. & Nedelkov, D. Mass spectrometric immunoassays for discovery, screening and quantification of clinically relevant proteoforms. *Bioanalysis* **8**, 1623–1633 (2016).
31. Rosàs-Canyelles, E., Modzelewski, A. J., Geldert, A., He, L. & Herr, A. E. Assessing heterogeneity among single embryos and single blastomeres using open microfluidic design. *Sci. Adv.* **6**, (2020).
32. Rosàs-Canyelles, E., Modzelewski, A., Geldert, A., He, L. & Herr, A. Multimodal detection of protein isoforms and nucleic acids from mouse pre-implantation embryos. *Nat. Protoc.* NP-PI200463 (2020). doi:10.1038/s41596-020-00449-2
33. Gkountela, S. *et al.* Circulating Tumor Cell Clustering Shapes DNA Methylation to Enable Metastasis Seeding. *Cell* **176**, 98-112.e14 (2019).
34. Pritzker, K. P. H. & Nieminen, H. J. Needle biopsy adequacy in the era of precision medicine and value-based health care. *Arch. Pathol. Lab. Med.* **143**, 1399–1415 (2019).
35. Lizotte, P. H. *et al.* Fine needle aspirate flow cytometric phenotyping characterizes immunosuppressive nature of the mesothelioma microenvironment. *Sci. Rep.* **6**, 1–8 (2016).
36. Tang, F. *et al.* RNA-Seq analysis to capture the transcriptome landscape of a single cell. *Nat. Protoc.* **5**, 516–535 (2010).
37. Grindberg, R. V. *et al.* RNA-sequencing From Single Nuclei. *Proc. Natl. Acad. Sci.* **110**, 19802–19807 (2013).
38. Abdelmoez, M. N. *et al.* SINC-seq: Correlation of transient gene expressions between nucleus and cytoplasm reflects single-cell physiology. *Genome Biol.* **19**, 1–11 (2018).
39. Kang, C. C. *et al.* Single cell-resolution western blotting. *Nat. Protoc.* **11**, 1508–1530 (2016).
40. Sinkala, E. *et al.* Profiling protein expression in circulating tumour cells using microfluidic western blotting. *Nat. Commun.* **8**, (2017).
41. Rosàs-Canyelles, E., Dai, T., Lia, S. & Herr, A. E. Mouse-to-

mouse variation in maturation heterogeneity of smooth muscle cells. *Lab Chip* **18**, 1875–1883 (2018).

42. Yamauchi, K. A. & Herr, A. E. Subcellular western blotting of single cells. *Microsystems Nanoeng.* **3**, (2017).
43. Hughes, A. J., Tentori, A. M. & Herr, A. E. Bistable isoelectric point photoswitching in green fluorescent proteins observed by dynamic immunoprobed isoelectric focusing. *J Am Chem Soc.* **134**, 17582–17591 (2012).
44. Alex J. Hughes *et al.* Single-cell western blotting. *Nat. Methods* **11**, 749–755 (2014).
45. Schwanhäusser, B. *et al.* Global quantification of mammalian gene expression control. *Nature* **473**, 337–342 (2011).
46. Kang, C.-C. *et al.* Single cell–resolution western blotting. *Nat. Protoc.* **11**, 1508–1530 (2016).
47. Schneider, C. A., Rasband, W. S. & Eliceiri, K. W. NIH Image to ImageJ : 25 years of image analysis HISTORICAL commentary NIH Image to ImageJ : 25 years of image analysis. *Nat. Methods* **9**, 671–675 (2012).
48. Lee, H. & Jin-Soo Kim. Unexpected CRISPR on-target effects. *Nat. Biotechnol.* **36**, 703–704 (2018).
49. Zischewski, J., Fischer, R. & Bortesi, L. Detection of on-target and off-target mutations generated by CRISPR/Cas9 and other sequence-specific nucleases. *Biotechnol. Adv.* **35**, 95–104 (2017).